Correlation between arabinose content and the conformation of arabinoxylan in water dispersions

Carbohydrate Polymers 368 (2025) 124082

Contents lists available at ScienceDirect

Carbohydrate Polymers

journal homepage: www.elsevier.com/locate/carbpol

Correlation between arabinose content and the conformation of arabinoxylan in water dispersions

Ratchawit Janewithayapun [a,b], Fabrice Cousin [c], Pamela Freire de Moura Pereira [d], Fátima Herranz-Trillo [e], Ann E. Terry [e], Jan Skov Pedersen [f], Amparo Jiménez-Quero [d], Anna Ström [a,b,*]

[a] Department of Chemistry and Chemical Engineering, Chalmers University of Technology, Gothenburg, SE-412 96, Sweden
[b] FibRe Center for Lignocellulose-based Thermoplastics, Chalmers University of Technology, Gothenburg, SE-412 96, Sweden
[c] Laboratoire Léon Brillouin, Université Paris-Saclay, UMR 12, CEA-CNRS, Gif Sur Yvette, 91191, France
[d] Department of Life Sciences, Chalmers University of Technology, Gothenburg, SE-412 96, Sweden
[e] MAX IV Laboratory, Lund University, Lund, SE-221 00, Sweden
[f] Department of Chemistry and Interdisciplinary Nanoscience Center, Aarhus University, Aarhus, 8000, Denmark

ARTICLE INFO

Keywords:
Wheat bran
Linkage analysis
NMR
Intrinsic viscosity
Monosaccharide analysis

ABSTRACT

Arabinoxylan (AX) with varying arabinose to xylose (A/X) ratios of 0.85, 0.57 and 0.39 was extracted from wheat bran, and the conformations of the AX polysaccharides dispersed in water were investigated using small-angle X-ray scattering. The persistence length (L_p) and the conformation statistics (expressed by the Flory exponent υ or the mass fractal) of the AX varied with their A/X ratios. The L_p decreased with decreasing A/X ratio, from 4.5 nm to 1.5 nm, where the AX with high and intermediate A/X ratios can be considered semi-flexible chains, while AX with the lowest A/X ratio behaves as a flexible chain. The mass fractal increased from 1.7 to 2.5 between the highest and lowest A/X ratios, indicating increasingly compact polymer conformations. AX with the highest A/X ratio behaved as chains in a good solvent and was well dispersed even in the semi-dilute regime. AX with intermediate and low A/X ratios showed stronger tendencies to aggregate and were not well dispersed at higher concentrations. The results presented show that the macroscopic properties of AX dispersions can be understood based on the chemical composition and fine structure of the AX polysaccharide.

1. Introduction

Arabinoxylan (AX) is a polysaccharide present in cereals such as wheat, maize, and rye, and is therefore consumed through a range of cereal-based foods. AX is available from side-streams generated by agro-industrial activities and bioethanol production (Solomou et al., 2022), where the use of AX as a food ingredient or starting point for material development is of interest. AX has been proposed for use as an ingredient in bread (Pietiäinen et al., 2024), a cryoprotectant (Fessas & Schiraldi, 2001) and a polymer for material applications (Börjesson et al., 2019; Jia et al., 2023).

The backbone of AX consists of β-(1→4)-D-xylopyranosyl units partially substituted with α-*L*-arabinofuranosyl on *O*-3 and/or *O*-2 of a xylose unit (Schooneveld-Bergmans et al., 1999). Both the conformation of the individual AX chains in dispersion and the extent of aggregation caused by intermolecular interactions determine the macromolecular properties of the dispersion. The polymer conformation relates to both the chain persistence length (L_p), and on the chains' conformation statistics, which is the chains' interaction with themselves and with the solvent. Experiments have shown that AX with lower arabinose to xylose (A/X) ratio show a tendency to interact and aggregate, as arabinose side chains have been suggested to help reduce intermolecular interactions (Andrewartha et al., 1979; Köhnke et al., 2011; Pitkänen et al., 2011). There is still, however, debate on whether the composition has an effect on the AX conformation, with studies having investigated the variation of the L_p of AX with differing A/X ratios (Man et al., 2021; Dervilly-Pinel et al., 2001; Pitkänen et al., 2009).

Dervilly-Pinel et al. (2001) showed that the conformation of wheat flour AX with different A/X ratios, did not vary. In other studies, it was shown that the composition and substitution pattern of AX led to differences in conformation: based on comparisons between wheat and rye AX (Pitkänen et al., 2009), and when the arabinose units of wheat AX were cleaved (Andrewartha et al., 1979; Köhnke et al., 2011).

* Corresponding author at: Department of Chemistry and Chemical Engineering, Chalmers University of Technology, Gothenburg, SE-412 96, Sweden.
E-mail address: anna.strom@chalmers.se (A. Ström).

https://doi.org/10.1016/j.carbpol.2025.124082
Received 11 May 2025; Received in revised form 7 July 2025; Accepted 16 July 2025
Available online 27 July 2025

Size exclusion chromatography with multi-angle light scattering (SEC-MALS) has been the most reported method for studying the conformation of AX. SEC-MALS can be used to characterize the quality of the chain-solvent interactions and to determine the L_p of the measured chains. Through this technique, a range of L_p values have been reported for AX, ranging from 2 nm to 8 nm (Andrewartha et al., 1979; Dervilly-Pinel et al., 2001; Picout & Ross-Murphy, 2002; Pitkänen et al., 2009). The analysis of SEC-MALS result is nontrivial and the obtained L_p vary depending on choice of model (Picout & Ross-Murphy, 2002). For wheat flour AX, L_p values of 6 nm to 8 nm (Dervilly-Pinel et al., 2001), and 3 nm to 5 nm (Picout & Ross-Murphy, 2002) were calculated for the same dataset, through two different analytical approaches. Another study reported L_p values close to 2 nm (Pitkänen et al., 2009), which would place AX as a fairly flexible polysaccharide, similar to pullulan (1.2 nm to 1.9 nm) (Muroga et al., 1987; Yang & Sato, 2020). The higher L_p values of 5 nm to 8 nm would describe AX as a semi-flexible polysaccharide (Dervilly-Pinel et al., 2001) similar to, for example, xyloglucan (~ 8 nm) (Muller et al., 2011).

Using small-angle neutron scattering (SANS), Petermann et al. (2023) obtained a fitting of wheat flour AX to a worm-like chain model with an L_p of 4.5 nm. This value is in agreement with another small-angle X-ray scattering (SAXS)/SANS study on AX from *Plantago ovata* seed by Yu et al. (2018), which also reported an L_p of 4.5 nm. An advantage with SAXS/SANS is that the L_p, solvent interaction and aggregation are represented by scattering features on different length-scales, all of which can be probed directly, allowing the decoupling of the chain conformation from aggregation effects. As such, SAXS/SANS techniques are placed in a good position to investigate polysaccharide conformation and aggregation in dispersions.

Here, we aim to clarify the impact of the A/X ratio on AX conformation in the different concentration regimes, and attempt to separate effects of A/X ratio on aggregation and solvent interactions, using SAXS. We build on, and extend the work done by Petermann et al. (2023), who used SANS to investigate the water conformation of one wheat flour AX material (with A/X ratio of 0.61). We investigate three AX polysaccharides extracted from wheat bran with A/X ratios of 0.39, 0.57 and 0.85.

2. Experimental

2.1. Materials

Wheat bran was kindly provided by Lantmännen (Sweden). Chemicals used for the extraction were purchased from Sigma-Aldrich (Schnelldorf, Germany). Ethanol (95%) was purchased from Solveco (Rosersberg, Sweden). β-glucanase (EC.2.1.73) from Bacillus Subtilis was purchased from Megazyme (Wicklow, Ireland). 72% H_2SO_4 was purchased from Chemlab (Zedelgem, Belgium), NaOH and NaOAc from Merck (Darmstadt, Germany), monosaccharide standards from Sigma-Aldrich (Schnelldorf, Germany). Dimethyl sulfoxide (DMSO) and LiBr were purchased from Sigma-Aldrich (Schnelldorf, Germany). Trifluoracetic acid (TFA), methyl iodine, dichloromethane, sodium borodeuteride, pyridine and acetic anhydride were purchased from Sigma-Aldrich (Schnelldorf, Germany) and 32% ammonia solution was purchased from Millipore (Stockholm, Sweden).

2.2. Extraction and fractionation of AX

AX was extracted from wheat bran through alkali extraction with $Na_2S_2O_4$ as the reducing agent, followed by fractionation with ethanol according to water solubility following the procedure in Janewithayapun et al. (2024). The AX fraction precipitated at 20% ethanol (AX0.39) contained β-glucan, which was degraded using β-glucanase (500 μL, 25 units) in sodium phosphate buffer solution (200 mL, 20 mM, pH 6.5).

2.3. Chemical composition of AX samples

Monosaccharide composition from the sulfuric acid hydrolysis procedure: The AX were hydrolyzed using the sulfuric acid procedure (Sluiter et al., 2008; Theander & Westerlund, 1986) and the resulting monosaccharides were analyzed using high-performance anion exchange chromatography with pulsed amperometric detection (HPAEC-PAD) as reported by Janewithayapun et al. (2024). Quantification was carried out against calibration curves built with neutral sugars (fucose, arabinose, rhamnose, galactose, glucose, xylose, and mannose). The acid soluble lignin content (ASL) was calculated from the UV absorbance at 205 nm of the hydrolyzates using the Specord 205 (Analytik Jena, Jena, Germany) (Jedvert et al., 2012). The insoluble content was measured from the weight of the filtered residues after drying overnight at 105 °C.

Monosaccharide composition from the TFA hydrolysis procedure: The monosaccharide composition was also characterized using the trifluoroacetic acid (TFA) hydrolysis procedure (Albersheim et al., 1967). AX were submitted to hydrolysis with 2 M TFA at 121 °C for 3 h. Determinations were performed using HPAEC-PAD (Dionex ICS-6000 system, Thermo Fischer, USA). A column CarboPacTM PA20 (3 × 150 mm) was used for separation at 0.4 mL min^{-1}. The gradient method consisting of Milli-Q water, 200 mM NaOH, and 100 mM NaOH + 100 mM NaOAc, as eluents. Quantification was carried out against calibration curves built with neutral sugars (as above) and uronic acids (galacturonic and glucuronic acids).

Quantification of arabinose to xylose ratio using NMR: The AX fractions were dissolved in DMSO-*d6* by heating at 70 °C followed by sonication for 30 min. ^1H and ^{13}C spectra were collected at 45 °C on an Oxford 800 MHz magnet, with the Bruker Avance III HD spectrometer equipped with a 5 mm TXO cryoprobe. The A/X ratio was quantified by integration of the arabinose C1 region (105.5–110 ppm) and the xylose C1 region (99–103.8 ppm).

Glycosidic linkage analysis: Glycosidic linkage analysis was performed on permethylated alditol acetates derivatized (PMAAs) samples using gas chromatography–mass spectrometery (GC–MS) analysis according to the method described by Pettolino et al. (2012), with small modifications. AX samples were swelled in anhydrous DMSO overnight, followed by addition of solid NaOH and methylation with methyl iodine in 5 cycles. The samples were partitioned with dichloromethane and water, dried, and submitted to hydrolysis with 2 M TFA at 121 °C for 3 h. Then, a reduction with 0.25 M sodium borodeuteride in 1 M ammonia was carried out, followed by acetylation with pyridine and acetic anhydride. The PMAAs were recovered and analyzed using a GC (Nexis GC-2030, Shimadzu, KYT, Japan) coupled to an electron ionization single quadrupole MS (GCMS-QP2020 NX, Shimadzu, KYT, Japan) equipped with a SP-2380 capillary column (30 m × 0.25 mm, Supelco). Samples were semi-quantified in comparison with standards on retention times and fragmentation profile.

2.4. Shear viscosity for determination of intrinsic viscosity and overlap concentration

The apparent viscosity of AX dispersions at different concentrations were determined using a DHR-3 rheometer (TA Instruments, Delaware, USA) at $T = 25$ °C. The geometry used was cone-plate with a diameter of 40 mm and an angle of 1.01°. The temperature was controlled using a Peltier Plate. A shear rate sweep with shear rates from 1 s^{-1} to 800 s^{-1} was performed for each sample, and the viscosity at a shear rate of 10 s^{-1} was used to graphically determine the intrinsic viscosity $[\eta]$ through the Huggins and Kraemer equations (Eqs. (1) and (2)), and to determine the overlap concentration (c*). Measurements were performed in duplicates.

$$\frac{\eta_{spec}}{c} = [\eta] + k_H[\eta]^2 c \quad (1)$$

and

$$\frac{\ln(\eta_{rel})}{c} = [\eta] + k_K[\eta]^2 c \quad (2)$$

where

$$\eta_{spec} = \frac{(\eta - \eta_s)}{\eta_s} \quad (3)$$

and

$$\eta_{rel} = \frac{\eta}{\eta_s} \quad (4)$$

where η_s represents the η of the solvent, in this case water.

2.5. Size exclusion chromatography (SEC)

The molar mass of the AX fractions were determined with size exclusion chromatography (SEC). The mobile phase was DMSO with 10 mM LiBr. A PL-HPC 50 Plus Integrated GPC system (Polymer Laboratories, Agilent, Santa Barbara, USA), was equipped with two 300 × 7.5 mm PolarGel-M columns and one 50 × 7.5 mm PolarGel-M guard column. Samples were prepared in the mobile phase at 2 mg mL^{-1}, heated at 70 °C for 15 min, then stirred overnight and filtered through a 0.2 μm syringe filter prior to injection. The flow rate was 0.5 mL min^{-1} at 50 °C, and the total injection volume was 100 μL. A DAWN multi-angle laser light scattering detector (Wyatt Technologies, Santa Barbara, U.S.) and a PL-RI refractive index detector (Polymer Laboratories, Agilent, Santa Barbara, USA) were used for detection. A dn/dc value of 0.064 mL g^{-1} was used (Goring & Timell, 1960). Measurements were compared against pullulan standards (Shodex P-82, Lot No. 220604, Showa Denko K.K., Tokyo, Japan). The ASTRA software for Windows (8.2.2) was used for data analysis.

2.6. Sample preparation for small-angle scattering

AX stock dispersions were prepared using deionized water at concentrations of 40 mg mL^{-1} for the AX containing the highest amount of arabinose, and 20 mg mL^{-1} for the intermediate and low arabinose containing samples. The dispersions were sonicated for 30 min, followed by heating at 80 °C for 30 min, then left stirring overnight at room temperature. Lower concentration dispersions of AX were obtained by dilution of concentrated stock dispersions for each material.

2.7. Synchrotron small-angle X-ray scattering (SAXS)

SAXS experiments were performed at the CoSAXS beamline at MAX IV laboratory. An X-ray wavelength (λ) of 1.0 Å was used, and detection was done simultaneously on the SAXS detector Eiger2 4M (Dectris AG, Switzerland) and the WAXS detector Pilatus3 2M (Dectris AG, Switzerland). The detectors were positioned at distances of 10.12 m (SAXS) and 0.57 m (WAXS) from the sample, covering a q range from 0.0013 $Å^{-1}$ to 0.94 $Å^{-1}$. Samples were exposed to the beam by injection into a flow capillary system using a BioSAXS autoloader. Data reduction was carried out using the python implementation of MatFRAIA (Jensen et al., 2022) for radial integration. The integrated data were normalized to the X-ray beam transmittance and averaged, following data rejection using correlation maps to exclude any effects of radiation damage or inhomogeneities in the sample. Background subtraction and scaling to water absolute intensities were carried out using Python programs in Jupyter Notebook.

2.8. Bench-scale SAXS

Complimentary SAXS measurements, and of the intermediate A/X ratio samples were performed on a Xeuss 2.0 instrument (Xenocs). A Cu α source with λ of 1.54 Å was used, and detection was done with a Pilatus3 detector (Dectris AG, Switzerland) at two sample to detector distances: at 2490 mm, with a collimated beam size of 0.5 mm × 0.5 mm, and at 340 mm, with a collimated beam size of 0.8 mm × 0.8 mm. This gives a q range of 0.0045 $Å^{-1}$ to 1.8 $Å^{-1}$. The scattering signals from the empty beam, empty capillary, and dark field were measured separately. These signals were then subtracted from the sample scattering, considering their relative transmission. The resulting values were normalized using the incident beam intensity to obtain the scattering measurements in absolute units (cm^{-1}). Additionally, a reference measurement of the solvent water was independently obtained and its contribution to the sample scattering was subtracted.

2.9. Pycnometry

The mass density of AX0.85 was measured using an AccuPyc II 1340 gas pycnometer (Micromeritics, Georgia, U.S.) with a 10 cm^3 cylindrical holder. Analysis was performed with helium gas at 19.5 psig, with five purging and ten analysis cycles performed for each measurement. The value of the mass density was then used to calculate the X-ray scattering length density (SLD) of AX.

3. Results and discussion

3.1. Chemical characterization and substitution pattern of AX fractions

The chemical composition, as determined by HPAEC of acid hydrolyzates (using TFA and H_2SO_4), confirm that the three fractions are composed of primarily AX with varying amount of side chain arabinose (Table 1). The AX with the highest and intermediate A/X ratio contained low amounts of galactose and glucose (< 8 wt%), whereas no galactose and glucose were detected in the sample with the lowest amount of arabinose. Galactose can be found substituted on the xylose backbone, while the majority of glucose present should be from β-glucan (Saulnier et al., 2007), which was removed from the lowest A/X fraction by β-glucanase treatment following work by Janewithayapun et al. (2024). All fractions contained < 2 wt% uronic acid, < 6 wt% insolubles, and < 4 wt% ASL. We cannot detect a trend of increasing or decreasing insolubles or ASL between the different fractions. The wt% of the different monosaccharides agreed within 5 wt% units between the two different hydrolyzate methods and chromatography equipment used. In addition, the A/X ratio determined by HPAEC show good agreement with those determined by ^{13}C NMR of un-hydrolyzed AX for the high and intermediate AX fractions, with a larger variation for the AX fraction with the lowest amount of arabinose. The ^{1}H and ^{13}C spectra are shown in Figure S1 of the supplementary information. The fractions will from now on be named after the average A/X ratio obtained from the three different methods, thus; AX0.39 AX0.57 and AX0.85.

Glycosidic linkage analysis was performed to define the substitution pattern of xylose and arabinose units (Table S1, supplementary information). An increase in the proportion of di-substituted (2,3,4-Xyl*p*) was observed with increasing arabinose content, from 0.7/10 Xyl units for AX0.39 to 1.5/10 Xyl units for AX0.85. The observed pattern is also accompanied by an increase in the oligomeric sidechain fractions characterized by 2-Ara*f* and 2-Xyl*p* (Rudjito et al., 2020). A higher content of terminal xylose units (t-Xyl*p*), was found in AX0.85 compared to AX0.39 and AX0.57, which may also be related to the more complex substitution patterns in AX0.85. Data from the linkage analysis was used to make schematics of possible structure for AX0.39, AX0.57 and AX0.85 shown in Figs. 1a–c.

3.2. Molar mass determination

The molar mass (M_w) and dispersity (M_w/M_n) of AX fractions are shown in Table 2. In our SEC-MALS chromatograms, all three AX fractions showed a multimodal distribution with three peaks (Figure S2, supplementary information), which may indicate incomplete separation of AX in the column. The two peaks at later elution times were used to determine the M_w and M_w/M_n of our AX. The peak at earlier elution time corresponded to M_w of ~ one million g mol^{-1} and gave low RI responses, therefore, we attribute them to larger aggregates

Table 1
Monosaccharide composition, uronic acid, acid soluble lignin (ASL) and insolubles, as determined using acid hydrolysis and HPAEC. The arabinose/xylose (A/X) ratio calculated from the HPAEC monosaccharide composition, and from ^{13}C NMR of non-hydrolyzed samples are also shown. *n.d. means that this component was not detected.*

Component (wt%)	AX0.39		AX0.57		AX0.85	
	H_2SO_4	TFA	H_2SO_4	TFA	H_2SO_4	TFA
Arabinose	28	26	29	33	42	43
Rhamnose	n.d.	n.d.	n.d.	n.d.	n.d.	n.d.
Galactose	n.d.	2	3	4	4	4
Glucose	n.d.	3	8	6	n.d.	1
Xylose	62	67	53	56	46	50
Mannose	n.d.	n.d.	n.d.	n.d.	n.d.	n.d.
Insolubles	6	–	4	–	5	–
ASL	3	–	3	–	4	–
GalA	–	0	–	1	–	1
GlcA	–	2	–	1	–	1
A/X ratio	0.45	0.39	0.55	0.58	0.90	0.86
A/X ratio from ^{13}CNMR	0.34		0.57		0.80	

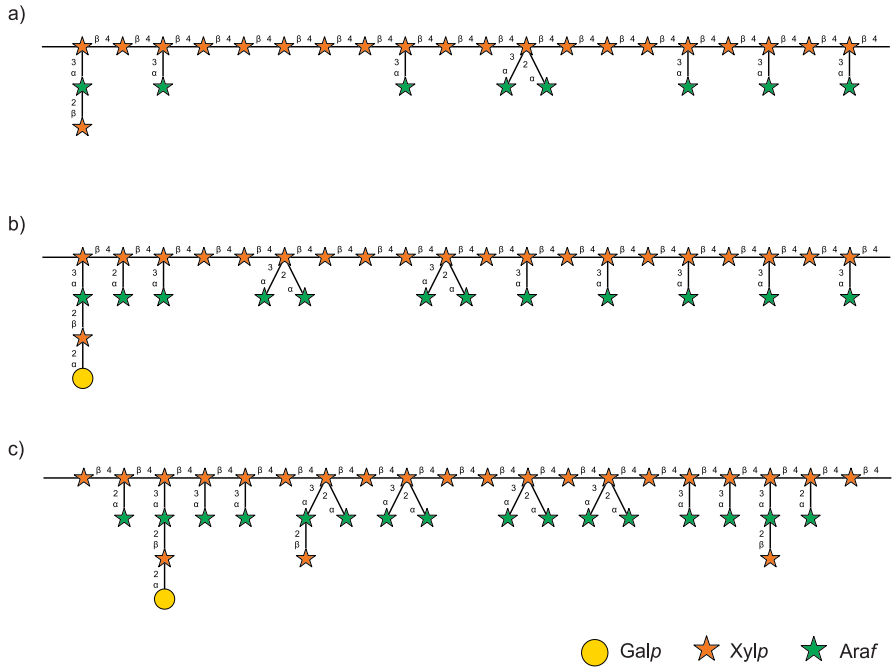

Fig. 1. Suggested structures of the fractionated arabinoxylans (a) AX0.39, (b) AX0.57, and (c) AX0.85 based on the monosaccharides and glycosidic linkage analysis and previous reports from: Rudjito et al. (2020), Bastos et al. (2018), Saulnier et al. (2013, 1995).

Table 2
Results from SEC-MALS analysis of AX in DMSO.

	Weight-averaged molar mass, M_w (kg mol^{-1})	Dispersity, M_w/M_n	z-averaged radius of gyration, R_g (nm)
AX0.39	120	1.9	22
AX0.57	170	2.0	30
AX0.85	220	1.6	33

(mass recoveries 5, 4 and 12% for AX0.39, AX0.57 and AX0.85) and this peak was omitted from the molar mass average calculations. The large aggregates could be related to undispersed AX clusters, or non-AX components such as protein. The peaks used for analysis contributed mass recoveries of 69, 66 and 71% for AX0.39, AX0.57 and AX0.85, respectively.

3.3. Intrinsic viscosity and overlap concentration

The [η] and the overlap concentration (c*) were determined through measurements of $\eta_{apparent}$ as a function of shear rate and concentration for AX0.85. Only AX0.85 was selected based on: (a) only AX0.85 gave transparent dispersions for the concentration range tested (Figure S3, supplementary information) and (b) the molar mass, and R_g were the highest for AX0.85 (Table 2). The c* obtained for AX0.85 should thus be the lowest among the three AX studied. The [η] of AX 0.85 was determined graphically through the Huggins–Kraemer plot (Fig. 2a), using AX concentrations between 2 to 7.5 mg mL^{-1}. The *y*-axis intercept from Huggins and Kraemer equations are 0.20 and 0.18 mL mg^{-1}, resulting in an average value of [η] of 0.19 mL mg^{-1}.

The η_{sp} of the AX0.85 dispersions were measured in the concentration range of 2 to 30 mg mL^{-1} and plotted as a function of reduced concentration (C[η]), shown in Fig. 2b. The value of c* of AX 0.85 was 7.9 mg mL^{-1}, which occurred at C[η] close to 1.5. This value of C[η] (1.5) is similar to the value of 1.2 as determined for AX from wheat flour (Petermann et al., 2023) and for xyloglucan (Muller et al., 2013). The slope of the η_{sp} as a function of C[η] was 1 in the dilute and 1.6 in the semi-dilute region. The values are close to those obtained for AX from mucilage (Yu et al., 2018), but lower than those reported for AX extracted from wheat flour and xyloglucan in the semi-dilute regime (2.1 and 2 respectively) (Muller et al., 2013; Petermann et al., 2023).

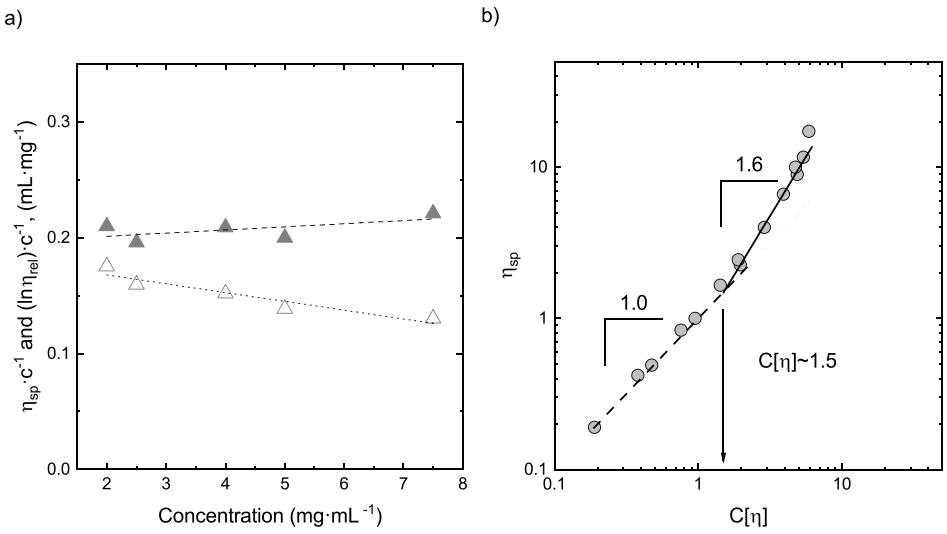

Fig. 2. (a) Huggins–Kraemer plot, filled symbols are values calculated according to Huggins eq. and open symbols are values calculated according to Kraemer eq. and (b) specific viscosity as a function of reduced concentration for AX0.85 measured at 25 °C.

From c* ∝ $M/(R_g^3)$ (Larson, 1999), we estimate the c* of AX0.57 and AX0.39 relative to AX0.85 using the values of M_w and R_g from SEC-MALS in Table 2. The c* of AX0.57 would be 1.03 times higher than that of AX0.85, and the c* AX0.39 would be 1.8 times higher than of AX0.85. Hence, all AX fractions are in their dilute regime at concentrations below 8 mg mL^{-1}.

3.4. Dependence of AX conformation on A/X ratio in dilute dispersions

AX0.39 and AX0.85 dispersions were measured at CoSAXS, MAX IV laboratory, while AX0.57 was measured on the bench-scale Xeuss 2.0 at concentrations representing dilute conditions (1 mg mL^{-1} and 4 mg mL^{-1}). As shown in Fig. 3a and in the scaled plot in Fig. 3b, the scattering profile of the AX dispersions at 1 mg mL^{-1} indicate dispersed AX chains, with contributions from some larger aggregates, irrespective of arabinose content.

At the highest q values, we observe scattering from the AX chains' cross-section (Muller et al., 2011), then, at around q = 0.2 Å^{-1} there is a cross-over to a ~ q^{-1} scaling characteristic of scattering from a rod-like object (Beaucage et al., 1997; Muller et al., 2011). From Fig. 3b, the more extended q^{-1} region for AX0.85 and AX0.57, down to $q \approx 0.05$ Å^{-1}, indicates that these samples have a longer L_p than AX0.39, which has the q^{-1} scaling ending at $q \approx 0.13$ Å^{-1} (Beaucage et al., 1997).

The intermediate q region refers to the q range in between the Guinier region and the q^{-1} region at high q. This is between $0.009 < q < 0.06$ Å^{-1} for AX0.85 and AX0.57, and $0.009 < q < 0.1$ Å^{-1} for AX0.39. At intermediate q, the AX conformation statistics are probed and it is possible to obtain the Flory exponent (υ) describing the interactions between the repeating units in an AX chain and the solvent from the scaling of the scattering intensity $q^{-1/\upsilon}$ (Muller et al., 2011; Rubinstein & Colby, 2003). AX0.85 has a scattering intensity that scales with $q^{-1.7}$ ($\upsilon \approx 0.59$) – indicating that AX0.85 behaves as an extended chain in a good solvent environment. The AX0.57 and AX0.39 have a scaling of $q^{-2.3 \text{ to } -2.5}$, which is indicative of a more compact structure, and therefore, poor AX–water interactions in comparison to AX0.85.

At lower q values ($q < 0.009$ Å^{-1}) the scattering intensity begins to level out into the Guinier region, where the radius of gyration (R_g) of a chain is probed. In this q range, we also observe contributions from larger aggregates in all samples ($q < 0.003$ Å^{-1}), even though the samples are dilute and visually transparent. The q exponent of the aggregates are lower (< 3) than the exponent obtained from wheat flour AX with A/X ratio of 0.61 by Petermann et al. (2023) (where the q exponent was 3.65), and occurs at lower q values, indicating a lower degree of aggregation and/or smaller average aggregate sizes in the case of the AX samples measured herein.

In the sections below, we perform a quantitative analysis of the scattering data obtained from the AX with different A/X ratio.

3.4.1. Conformation of AX with higher arabinose content

The scattering profile of AX0.85 at 1 mg mL^{-1} was fitted to a flexible cylinder model (Pedersen & Schurtenberger, 1996, 2004) with additional terms to account for deviations from the flexible cylinder model at high and low q (Eq. (5)). At low q, a power law term was added as a structure factor, accounting for deviations coming from aggregate contributions. A and n are fitting constants describing the power law background, and a factor of 0.01 was added for numerical stability reasons. In the second term of Eq. (5), a Gaussian chain function (Debye, 1947), with radius of gyration $R_{g,mol}$ and scale factor B, was added as a fluctuating term representing molecular scattering from the arabinose or xylose units at high q (Pedersen & Svaneborg, 2002; Westberry et al., 2022). $P_{sc}(q)$ is the single chain form factor, given by the scattering functions of excluded volume chains, $P_{chain}(q)$ and $P_{rod}(q)$, with interpolation and correction factors $\chi(q, L, b)$ and $\Gamma(q, L, b)$ (Eq. (7)). $S_{xs}(q)$ is the cross-section scattering function representing the flexible cylinder model, where R_{XS} is the cylinder cross section radius and $B_1(x)$ is the Bessel function of first kind and first order (Pedersen & Schurtenberger, 2004). Lastly, bkg is the q-independent background.

$$I(q) = I_0 P_{sc}(q) S_{xs}(q)\left(1 + A\left(\frac{0.01}{q}\right)^n\right) + \frac{I_0}{B}\left(\frac{2\left[\exp(-Z) + Z - 1\right]}{Z^2} - P_{sc}(q)S_{xs}(q)\right) + bkg \quad (5)$$

$$Z = (qR_{g,mol})^2 \quad (6)$$

$$P_{sc}(q) = [P_{chain}(q)(1 - \chi(q, L, b)) + P_{rod}(q)\chi(q, L, b)]\Gamma(q, L, b) \quad (7)$$

$$S_{xs}(q) = \left[\frac{2B_1(qR_{xs})}{qR_{xs}}\right]^2 \quad (8)$$

The low-q region, high q region, and fit results are shown in Fig. 4. Model fitting was performed using the WLSQSAXS program (Oliveira JCP and Pedersen JS, unpublished) (Pedersen, 1997). Full model parameters are presented in Table S2-S3 of the supplementary information. The model in Eq. (5), provides a good fit to the data, with

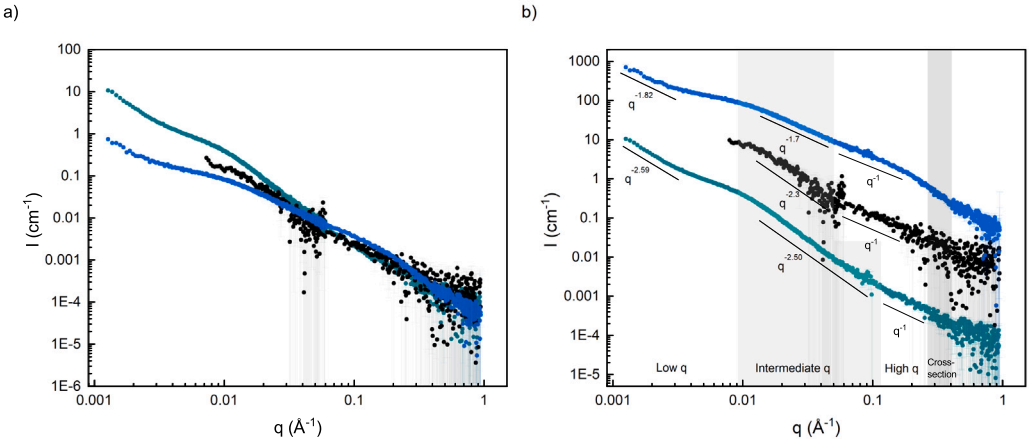

Fig. 3. (a) SAXS data from dispersions at 1 mg mL^{-1} for AX0.39 (green), AX0.57 (black), AX0.85 (blue), and (b) data scaled by factors of 1, 50, and 1000 for AX0.39, AX0.57, AX0.85 respectively for readability.

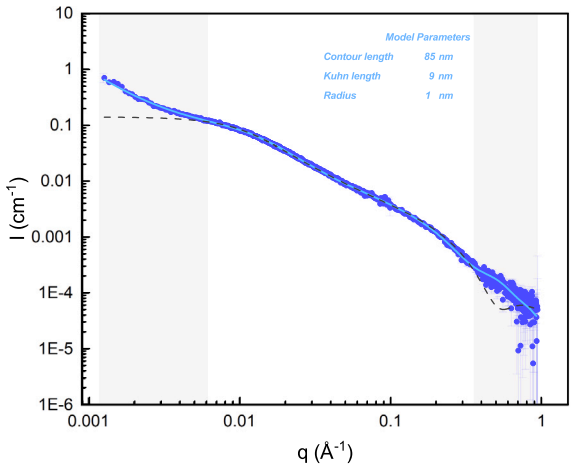

Fig. 4. Flexible cylinder fit to AX0.85 at 1 mg mL^{-1}. Blue line and text are the fitted results to the model in Eq. (5), the black dashed line represents fitting to a flexible cylinder model in SASView 5.0.5 (Alina et al., 2022).

a reduced chi-squared (χ^2_{red}) value of 1.41. The cross-section radius (R_{xs}) was obtained as 1.0 ± 0.03 nm, and Kuhn length (b) as 9.0 ± 0.3 nm. Using the general relation $b = 2L_p$ (Beaucage et al., 1997), the obtained L_p is 4.5 nm, similar to literature values of AX obtained from neutron scattering (Petermann et al., 2023; Yu et al., 2018). The contour length was obtained as 85 ± 2.3 nm, corresponding to an R_g of 11.2 nm (Pedersen & Schurtenberger, 2004).

3.4.2. Conformation of AX with intermediate arabinose content

The scattering data of AX0.57 cannot be fully represented with either the flexible cylinder model, with or without excluded volume effects (Pedersen & Schurtenberger, 1996), implemented in SASfit (Breßler et al., 2015) or the polymer chain with excluded volume effects model (Hammouda, 1993) as shown in Figs. 5a–b. As such, the AX0.57 can be reasoned to behave as a semi-flexible polysaccharide, owing to the relatively longer L_p, but with chains that are not fully extended in water, possibly having denser regions with stronger intra- or inter-molecular interactions.

The intermediate q decay of AX0.57 was approximately $q^{-2.3}$, as seen when the scattering intensity was fitted with the polymer chain model using a Porod exponent of 2.3 (Figs. 5a–b). The L_p can be roughly estimated from the point where the transition from q^{-1} to $q^{-2.3}$ occurs using the relation $L_p = 6/\pi q$ (Beaucage et al., 1997; Glatter, 1982), here with a transition $q \approx 0.05$ Å^{-1}. This gives an apparent L_p of 3.8 nm. Only an apparent L_p can be obtained, as the existence of intra- or inter-chain aggregation at local scales could cause the observed L_p to differ from the true L_p of a completely dispersed chain. Lastly, the R_g was estimated from fit of the polymer chain with excluded volume model to the 4 mg mL^{-1} sample as 21.6 ± 0.2 nm (Table S4, supplementary information).

3.4.3. Conformation of AX with lower arabinose content

The scattering intensity of AX0.39 was fitted with the polymer chain with excluded volume model (Hammouda, 1993), modified to include a power law term at low q, shown in Eq. (9), where $P_{exc}(q)$ is the polymer excluded volume form factor. Fitting was performed with the least_squares function in SciPy (version 1.14.1). Given the shorter q^{-1} region in AX0.39, only small deviations occurred in the high q region when fitted using this simpler model, and $\chi^2_{red} = 2.37$ (Fig. 6, with model parameters in Table S5 of the supplementary information). The fit resulted in an intermediate q decay of $q^{-2.50}$ ($v = 0.40$), and an R_g of 19.9 ± 0.1 nm. The apparent L_p of AX0.39 can be estimated with the same method used for AX0.57, with a transition at around $q = 0.13$ Å^{-1}, corresponding to an L_p of 1.5 nm. This would indicate that at lower A/X ratios, the xylan backbone has a higher freedom of movement. For the same reasons as the AX0.57, an apparent L_p is given for the AX0.39.

$$I(q) = scale \cdot P_{exc}(q)\left(1 + A\left(\frac{1}{q}\right)^n\right) + bkg \quad (9)$$

The results presented so far show that AX polysaccharides with increasing A/X ratios adopt more extended conformations in aqueous dispersions. The extended conformation was shown to be a result of changes in the L_p, and in the chains' conformation statistics. The L_p, which increased from an apparent value of 1.5 nm in AX0.39, to 4.5 nm in AX0.85 indicate that the average local chain segment of AX0.85 was stiffer than that of AX0.39. The intermediate q decay exponent ($1/v$) representing the conformation statistics, changed from partially collapsed polymer chains in poor solvent (AX0.39 and AX0.57) to that of chains in good solvent conditions (AX0.85). The lower apparent L_p in AX0.39 may be correlated to the higher amount of unsubstituted xylose residues present in this fraction (Fig. 1 and Table S1, supplementary information). Our results agree with observations where higher degree of substitutions of arabinose on the xylose backbone have been shown to reduce inter-molecular interactions in AX (Andrewartha et al., 1979; Köhnke et al., 2011), allowing AX to interact more favorably with water.

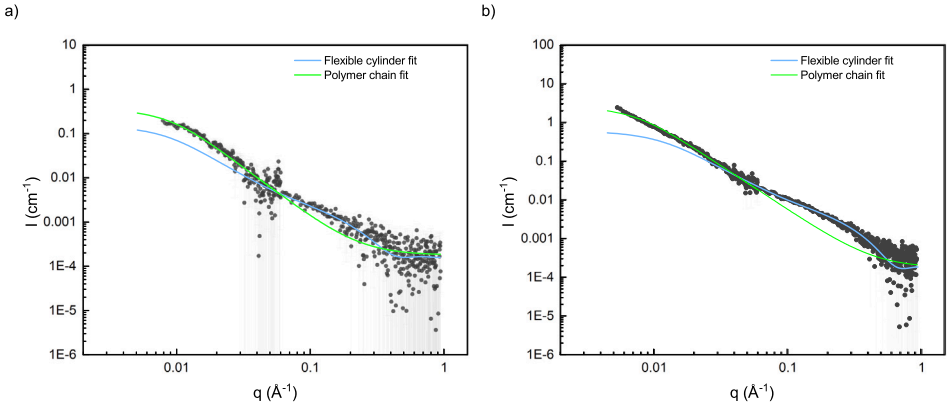

Fig. 5. Fitting of the AX0.57 scattering data with the polymer chain with excluded volume model (green) and the flexible cylinder model without excluded volume (blue), (a) at 1 mg mL^{-1}, and (b) at 4 mg mL^{-1}.

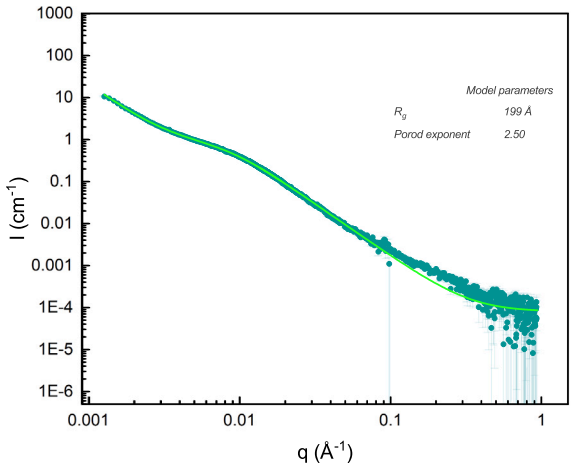

Fig. 6. Polymer chain with excluded volume model fitted to the scattering data of AX0.39.

3.5. Concentration effects on AX scattering profiles

AX0.85, AX0.57 and AX0.39 were macroscopically different from each other at higher concentrations (20 mg mL^{-1}), and also exhibited different behaviors when diluted to lower concentrations. At 20 mg mL^{-1}, AX0.39 was colloidally stable but turbid, indicating the existence of micrometer-sized aggregates (Figure S4, supplementary information). Dispersions of AX0.57 at 20 mg mL^{-1} were less turbid than AX0.39. Higher concentration dispersions of AX0.85 were instead transparent, indicating good dispersion (Figure S4, supplementary information). The macroscopic differences were also reflected in the scaling of the scattering intensities with concentration.

3.5.1. Concentration effects of AX with higher arabinose content

AX0.85 exhibits scaling behavior similar to those exhibited by polymer solutions (Thompson & Ryan, 2025), shown as a decrease in the scattering intensity at low q when normalized to concentration (Figs. 7a–b). This is more clearly seen in the plot of data normalized to the same intensity at high q, shown in Fig. 7b (Pedersen & Schurtenberger, 2004). The scale factor obtained from this normalization should represent the relative true concentration of AX0.85 dispersed in solution, shown in Fig. 7c.

From the shift in q of the Guinier plateau, the correlation length ξ is observed, which is related to R_g of the chains under dilute conditions by $\xi = R_g/\sqrt{3}$ (Pedersen & Schurtenberger, 2004). Above c*, ξ is the correlation length of the networks of interpenetrating AX chains (Pedersen & Schurtenberger, 2004). Furthermore, the intensity at $I(0)$ is inversely proportional to osmotic compressibility, and therefore, related to the second virial coefficient (A_2) by $I(0) \approx 1-2cMA_2$ (Pedersen & Schurtenberger, 2004), where M is the molar mass and c is the concentration. As such, by analyzing the concentration dependence of the scattering intensity of AX0.85, we obtain a description of its solvent quality.

Following the approach in Pedersen and Schurtenberger (2004), we use the polymer reference interaction site model (PRISM) model with a rod form factor for the screening correlation function $c(q, L_{\mathrm{PRISM}})$ where L_{PRISM} is the length of the rod form factor. The PRISM model scaling is applied to the first and second term describing the flexible cylinder and power law background in Eq. (5), the remaining terms are unchanged. The first and second terms from Eq. (5) become

$$\frac{\text{'Chain and aggregate form factor'}}{1+\beta c(q)P_{\mathrm{sc}}(q)} \tag{10}$$

where β is also a fitted parameter, and $\beta = 2MA_2c$. The full model is given in Eq. S2-S3 of the supplementary information.

Model fitting was performed using the WLSQSAXS program (Pedersen, 1997). The Kuhn length and contour length were fixed to the value obtained at the most dilute concentration of 0.25 mg mL^{-1}, and the other parameters were fitted. The model follows the trend of the concentration dependent behavior well (Fig. 7a), χ^2_{red} was between 1 to 3 in the concentration range 0.25 mg mL^{-1} to 1 mg mL^{-1}. The other concentrations had χ^2_{red} between 12.7 to 16, except for 20 mg mL^{-1}, which had a χ^2_{red} of 37.5. AX0.85 appears subject to small concentration effects even at 0.5 mg mL^{-1} and 1 mg mL^{-1}, as the fitted β was not zero (Fig. 7d). From a linear fit of β against concentration from scale factor, we obtain the second virial coefficient from the slope as $A_2 = 54.4M$ (with c in units of g mL^{-1}). Using $M = 220000$ g mol^{-1} from SEC-MALS, we obtain $A_2 = 0.00025$ mol mL g^{-2}, where a positive A_2 is expected from a polymer chain in good solvent conditions (Lindner, 2002).

The concentration derived from the SAXS intensity was used to evaluate β since there is some deviation from the expected concentration at 30 mg mL^{-1} and 40 mg mL^{-1} (Fig. 7c). As every sample was made by diluting the 40 mg mL^{-1} stock solution, it is possible that the deviation is a result of incomplete dispersion of AX chains at higher concentrations. This may also be related to the increasing scale and exponent of the low q power law term (Figure S5). The lower concentrations show good agreement between the targeted concentration and the scale factor, hence there may be concentration dependent interactions in AX0.85 similar to those observed in xyloglucans (Muller et al., 2013).

3.5.2. Concentration effects of AX with medium and low arabinose content

Both AX0.57 and AX0.39 did not disperse as well as AX0.85 did, instead showing trends towards forming larger structures at higher concentrations (Figs. 8 and 9). For AX0.57 at 20 mg mL^{-1}, the intermediate

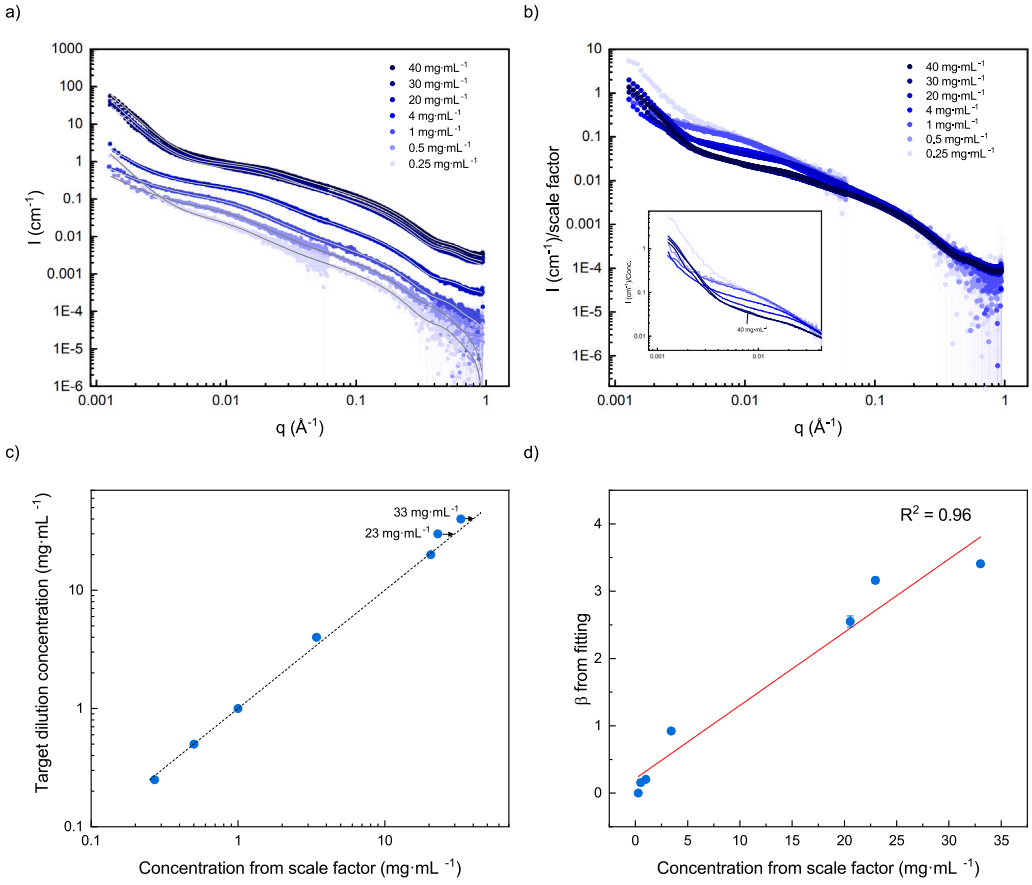

Fig. 7. (a) Scattering data of AX0.85 at different concentrations, (b) normalized scattering data for AX0.85 using the intensity at high q, with insert showing a magnified plot of the low q region. (c) Plot of target concentration from dilution against concentration obtained from the SAXS intensity scale factor. Labels indicate the scale factor, and the dashed line is the diagonal to aide interpretation. (d) Plot of β against concentration obtained from the scale factor. The red line is a linear fit where the slope $= 2MA_2$.

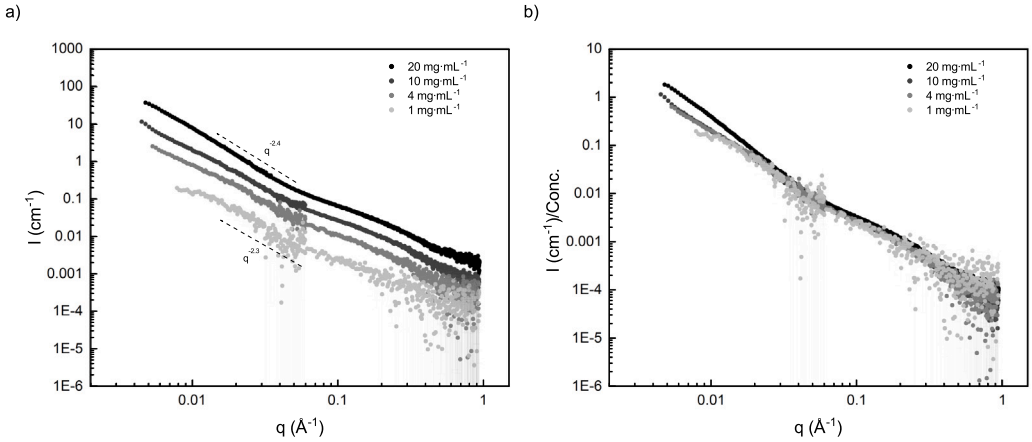

Fig. 8. (a) Scattering data of AX0.57 at different concentrations, (b) concentration normalized scattering data.

q exponent is $\sim q^{-2.4}$, and the shoulder around $q = 0.01$ Å^{-1} is weakly observed. When diluted to concentrations of 10, 4 and 1 mg mL^{-1}, we observe that the intermediate q exponent decreases to $q^{-2.3}$. Between 10, 4 and 1 mg mL^{-1}, no significant concentration dependence were detected (Figs. 8b). This implies that interactions leading to aggregation increases at higher concentrations, and are weaker at lower concentrations.

For AX0.39 we observed steeper q decays of $q^{-2.75}$ in the intermediate q region for the 20 mg mL^{-1} and 7.5 mg mL^{-1} sample, compared to the 1 mg mL^{-1} sample with decay of $q^{-2.50}$ (Fig. 9a–b). The shoulder at $q = 0.01$ Å^{-1} is also less pronounced at 20 mg mL^{-1} and stretches to lower q with a q^{-2} decay. The changes to the q exponents upon dilution are larger for AX0.39 than for AX0.57, which would correlate to a higher tendency for aggregation or network formation in AX0.39. AX0.39 seems to also be more difficult to disassociate than AX0.57, as the AX0.39 at 7.5 mg mL^{-1} sample behaved similarly to the 20 mg mL^{-1} sample, whereas for AX0.57, changes in aggregation behavior were observed already at 10 mg mL^{-1}. We find that the concentration dependent behavior of the AX fractions agree with, and further support the hypothesis that arabinose side groups

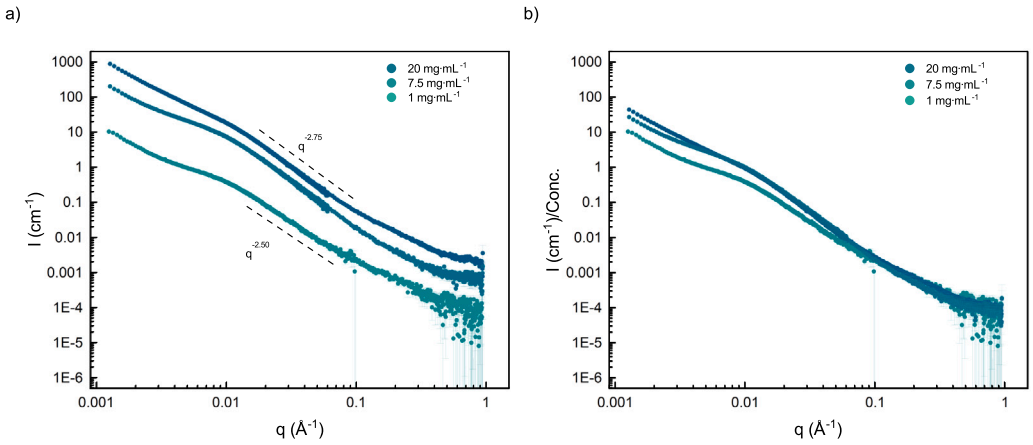

Fig. 9. (a) Scattering data of AX0.39 at different concentrations, (b) concentration normalized scattering data.

play an important role in preventing inter-molecular interactions in AX (Andrewartha et al., 1979; Pitkänen et al., 2011).

4. Conclusions

The conformation in water for AX0.85 was identified as that of a flexible cylinder in a good solvent environment, with L_p and contour length of 4.5 nm and 85 nm, respectively. The aggregate contributions in AX0.85 was low, and the single chain form factor could be well observed. AX0.57, with intermediate A/X ratio, exhibited an L_p of 3.8 nm which is close to that of AX0.85, however its solvent interaction with water was poor. The AX0.39, which had the lowest A/X ratio had the shortest L_p of 1.5 nm, and similarly poor interaction with water. Therefore, a higher A/X ratio of AX was correlated with a longer L_p and better solvent interactions with water.

The concentration dependence was investigated by studying the concentration series of each AX. AX0.85 exhibited scaling reminiscent to that of polymer solutions in good solvent conditions. We showed that the scattering intensity of AX0.85 could be described at all q regions using a polymer reference interaction site model (PRISM) structure factor. In contrast, AX0.39 and AX0.57 were not dispersed at higher concentrations, forming larger structures or aggregates, pointing towards the role of arabinose substitutions in reducing the inter-molecular interactions of AX. This understanding is helpful in the prediction of the macromolecular properties of AX dispersions based on their substitution characteristics.

CRediT authorship contribution statement

Ratchawit Janewithayapun: Writing – original draft, Methodology, Investigation, Formal analysis. **Fabrice Cousin:** Writing – review & editing, Supervision, Investigation, Formal analysis, Conceptualization. **Pamela Freire de Moura Pereira:** Writing – review & editing, Investigation. **Fátima Herranz-Trillo:** Methodology. **Ann E. Terry:** Writing – review & editing, Methodology, Formal analysis. **Jan Skov Pedersen:** Writing – review & editing, Methodology, Formal analysis. **Amparo Jiménez-Quero:** Writing – review & editing, Investigation, Formal analysis. **Anna Ström:** Writing – review & editing, Supervision, Funding acquisition, Formal analysis, Conceptualization.

Funding sources

We acknowledge the financial contribution from Formas – Swedish Research Council for Sustainable Development, with grant numbers 2020-01235, 2020-02843, Lantmännen foundation, with grant number 2020H064, and the Marie Skłodowska-Curie, with grant number 101107449.

Declaration of competing interest

The authors declare the following financial interests/personal relationships which may be considered as potential competing interests: Ratchawit Janewithayapun reports financial support was provided by Swedish Research Council Formas. If there are other authors, they declare that they have no known competing financial interests or personal relationships that could have appeared to influence the work reported in this paper.

Acknowledgments

The authors are grateful to the Division of Forest Products and Chemical Engineering at Chalmers for access to instruments for monosaccharide analysis, J. Ytterberg and P. Skansen for assistance with SEC-MALS, and to the Swedish NMR centre in Gothenburg for access to NMR spectrometers. We acknowledge MAX IV Laboratory for time on beamline CoSAXS under Proposal 20221186 and 20231013. Research conducted at MAX IV, a Swedish national user facility, is supported by the Swedish Research council under contract 2018-07152, the Swedish Governmental Agency for Innovation Systems under contract 2018-04969, and Formas under contract 2019-02496.

Appendix A. Supplementary data

Supplementary material related to this article can be found online at https://doi.org/10.1016/j.carbpol.2025.124082.

Data availability

Data will be made available on request.

References

Albersheim, P., Nevins, D. J., English, P. D., & Karr, A. (1967). A method for the analysis of sugars in plant cell-wall polysaccharides by gas-liquid chromatography. *Carbohydrate Research*, *5*(3), 340–345. http://dx.doi.org/10.1016/S0008-6215(00)80510-8.

Alina, G., Attala, Z., Bakker, J., Beaucage, P., Bourne, R., Bouwman, W., Breßler, I., Butler, P., Caddy-Jones, I., Campbell, K., Cho, J.-H., Cooper-Bennun, T., Hernandez, R. C., Doucet, M., Doutch, J., Durniak, C., Forster, L., Gilbert, P., Gonzalez, M., ... Zhou, J. (2022). SASView (version 5.0.5) [Computer software]. https://www.sasview.org/.

Andrewartha, K. A., Phillips, D. R., & Stone, B. A. (1979). Solution properties of wheat-flour arabinoxylans and enzymically modified arabinoxylans. *Carbohydrate Research*, *77*(1), 191–204.

Bastos, R., Coelho, E., & Coimbra, M. A. (2018). 8 - Arabinoxylans from cereal by-products: Insights into structural features, recovery, and applications. In C. M. Galanakis (Ed.), *Woodhead publishing series in food science, technology and nutrition*, *Sustainable recovery and reutilization of cereal processing by-products* (pp. 227–251). Woodhead Publishing, http://dx.doi.org/10.1016/B978-0-08-102162-0.00008-3.

Beaucage, G., Rane, S., Sukumaran, S., Satkowski, M. M., Schechtman, L. A., & Doi, Y. (1997). Persistence length of isotactic poly(hydroxybutyrate). *Macromolecules*, *30*(14), 4158–4162. http://dx.doi.org/10.1021/ma970373t.

Börjesson, M., Westman, G., Larsson, A., & Ström, A. (2019). Thermoplastic and flexible films from arabinoxylan. *ACS Applied Polymer Materials*, *1*(6), 1443–1450. http://dx.doi.org/10.1021/acsapm.9b00205.

Breßler, I., Kohlbrecher, J., & Thünemann, A. F. (2015). *SASfit*: a tool for small-angle scattering data analysis using a library of analytical expressions. *Journal of Applied Crystallography*, *48*(5), 1587–1598. http://dx.doi.org/10.1107/S1600576715016544.

De Man, W. L., Vaneeckhaute, E., De Brier, N., Wouters, A. G., Martens, J. A., Breynaert, E., & Delcour, J. A. (2021). 1H diffusion-ordered nuclear magnetic resonance spectroscopic analysis of water-extractable arabinoxylan in wheat (Triticum aestivum L.) flour. *Journal of Agricultural and Food Chemistry*, *69*(13), 3912–3922.

Debye, P. (1947). Molecular-weight determination by light scattering. *The Journal of Physical and Colloid Chemistry*, *51*(1), 18–32. http://dx.doi.org/10.1021/j150451a002.

Dervilly-Pinel, G., Thibault, J.-F., & Saulnier, L. (2001). Experimental evidence for a semi-flexible conformation for arabinoxylans. *Carbohydrate Research*, *330*(3), 365–372. http://dx.doi.org/10.1016/S0008-6215(00)00300-1.

Fessas, D., & Schiraldi, A. (2001). State diagrams of arabinoxylan-water binaries. *Thermochimica Acta*, *370*(1), 83–89. http://dx.doi.org/10.1016/S0040-6031(00)00783-8.

Glatter, O. (1982). *Small Angle X-ray Scattering* (pp. 363–385). Academic Press.

Goring, D. A. I., & Timell, T. E. (1960). Molecular properties of six 4-o-methylglucuronoxylans. *Journal of Physical Chemistry*, *64*(10), 1426–1430. http://dx.doi.org/10.1021/j100839a015.

Hammouda, B. (1993). SANS from homogeneous polymer mixtures: A unified overview. In *Polymer characteristics* (pp. 87–133). Berlin, Heidelberg: Springer Berlin Heidelberg, http://dx.doi.org/10.1007/BFb0025862.

Janewithayapun, R., Hedenqvist, M. S., Cousin, F., Idström, A., Evenäs, L., Lopez-Sanchez, P., Westman, G., Larsson, A., & Ström, A. (2024). Nanostructures of etherified arabinoxylans and the effect of arabinose content on material properties. *Carbohydrate Polymers*, *331*, Article 121846. http://dx.doi.org/10.1016/j.carbpol.2024.121846.

Jedvert, K., Saltberg, A., Theliander, H., Wang, Y., Henriksson, G., & Lindström, M. E. (2012). BIOREFINERY: Mild steam explosion: A way to activate wood for enzymatic treatment, chemical pulping and biorefinery processes. *Nordic Pulp & Paper Research Journal*, *27*(5), 828–835.

Jensen, A. B., Christensen, T. E. K., Weninger, C., & Birkedal, H. (2022). Very large-scale diffraction investigations enabled by a matrix-multiplication facilitated radial and azimuthal integration algorithm: MatFRAIA. *Journal of Synchrotron Radiation*, *29*(6), 1420–1428.

Jia, S., Lv, Z., Rao, J., Lü, B., Chen, G., Bian, J., Li, M., & Peng, F. (2023). Xylan plastic. *ACS Nano*, *17*(14), 13627–13637. http://dx.doi.org/10.1021/acsnano.3c02327.

Köhnke, T., Östlund, Å., & Brelid, H. (2011). Adsorption of arabinoxylan on cellulosic surfaces: Influence of degree of substitution and substitution pattern on adsorption characteristics. *Biomacromolecules*, *12*(7), 2633–2641. http://dx.doi.org/10.1021/bm200437m.

Larson, R. G. (1999). Intrinsic viscosity and overlap concentration. In *Topics in chemical engineering, The structure and rheology of complex fluids* (pp. 113–114). New York: Oxford University Press.

Lindner, P. (2002). Chapter 2 - scattering experiments: Experimental aspects, initial data reduction and absolute calibration. In *Neutrons, x-rays and light: scattering methods applied to soft condensed matter* (pp. 23–48). Elsevier.

Muller, F., Jean, B., Perrin, P., Heux, L., Boué, F., & Cousin, F. (2013). Mechanism of associations of neutral semiflexible biopolymers in water: The xyloglucan case reveals inherent links. *Macromolecular Chemistry and Physics*, *214*(20), 2312–2323. http://dx.doi.org/10.1002/macp.201300265.

Muller, F., Manet, S., Jean, B., Chambat, G., Boué, F., Heux, L., & Cousin, F. (2011). SANS measurements of semiflexible xyloglucan polysaccharide chains in water reveal their self-avoiding statistics. *Biomacromolecules*, *12*(9), 3330–3336. http://dx.doi.org/10.1021/bm200881x.

Muroga, Y., Yamada, Y., Noda, I., & Nagasawa, M. (1987). Local conformation of polysaccharides in solution investigated by small-angle x-ray scattering. *Macromolecules*, *20*(12), 3003–3006. http://dx.doi.org/10.1021/ma00178a009.

Pedersen, J. S. (1997). Analysis of small-angle scattering data from colloids and polymer solutions: modeling and least-squares fitting. *Advances in Colloid and Interface Science*, *70*, 171–210. http://dx.doi.org/10.1016/S0001-8686(97)00312-6.

Pedersen, J. S., & Schurtenberger, P. (1996). Scattering functions of semiflexible polymers with and without excluded volume effects. *Macromolecules*, *29*(23), 7602–7612.

Pedersen, J. S., & Schurtenberger, P. (2004). Scattering functions of semidilute solutions of polymers in a good solvent. *Journal of Polymer Science Part B: Polymer Physics*, *42*(17), 3081–3094.

Pedersen, J. S., & Svaneborg, C. (2002). Scattering from block copolymer micelles. *Current Opinion in Colloid & Interface Science*, *7*(3), 158–166. http://dx.doi.org/10.1016/S1359-0294(02)00044-4.

Petermann, M., Dianteill, L., Zeidi, A., Vaha Ouloassekpa, R., Budisavljevic, P., Le Men, C., Montanier, C., Roblin, P., Cabane, B., Schweins, R., Dumon, C., & Bouchoux, A. (2023). Arabinoxylan in water through SANS: Single-chain conformation, chain overlap, and clustering. *Biomacromolecules*, *24*(8), 3619–3628. http://dx.doi.org/10.1021/acs.biomac.3c00374.

Pettolino, F. A., Walsh, C., Fincher, G. B., & Bacic, A. (2012). Determining the polysaccharide composition of plant cell walls. *Nature Protocols*, *7*(9), 1590–1607.

Picout, D. R., & Ross-Murphy, S. B. (2002). On the chain flexibility of arabinoxylans and other $\beta-(1-4)$ polysaccharides. *Carbohydrate Research*, *337*(19), 1781–1784. http://dx.doi.org/10.1016/S0008-6215(02)00281-1.

Pietiäinen, S., Jimenez-Quero, A., Moldin, A., Ström, A., Katina, K., & Langton, M. (2024). Feruloylation and hydrolysis of arabinoxylan extracted from wheat bran: Effect on bread quality and shelf-life. *Journal of Cereal Science*, *117*, http://dx.doi.org/10.1016/j.jcs.2024.103920.

Pitkänen, L., Tuomainen, P., Virkki, L., & Tenkanen, M. (2011). Molecular characterization and solution properties of enzymatically tailored arabinoxylans. *International Journal of Biological Macromolecules*, *49*(5), 963–969. http://dx.doi.org/10.1016/j.ijbiomac.2011.08.020.

Pitkänen, L., Virkki, L., Tenkanen, M., & Tuomainen, P. (2009). Comprehensive multidetector HPSEC study on solution properties of cereal arabinoxylans in aqueous and DMSO solutions. *Biomacromolecules*, *10*(7), 1962–1969.

Rubinstein, M., & Colby, R. H. (2003). Polymer physics. (pp. 97–126). Oxford University Press, http://dx.doi.org/10.1093/oso/9780198520597.001.0001.

Rudjito, R. C., Jiménez-Quero, A., Hamzaoui, M., Kohnen, S., & Vilaplana, F. (2020). Tuning the molar mass and substitution pattern of complex xylans from corn fibre using subcritical water extraction. *Green Chemistry*, *22*(23), 8337–8352.

Saulnier, L., Guillon, F., Sado, P.-E., Chateigner-Boutin, A. L., & Rouau, X. (2013). Plant cell wall polysaccharides in storage organs: xylans (food applications). *Reference Module in Chemistry, Molecular Sciences and Chemical Engineering*, np.

Saulnier, L., Sado, P.-E., Branlard, G., Charmet, G., & Guillon, F. (2007). Wheat arabinoxylans: exploiting variation in amount and composition to develop enhanced varieties. *Journal of Cereal Science*, *46*(3), 261–281.

Saulnier, L., Vigouroux, J., & Thibault, J.-F. (1995). Isolation and partial characterization of feruloylated oligosaccharides from maize bran. *Carbohydrate Research*, *272*(2), 241–253. http://dx.doi.org/10.1016/0008-6215(95)00053-V.

Schooneveld-Bergmans, M., Beldman, G., & Voragen, A. (1999). Structural features of (glucurono) arabinoxylans extracted from wheat bran by barium hydroxide. *Journal of Cereal Science*, *29*(1), 63–75.

Sluiter, A., Hames, B., Ruiz, R., Scarlata, C., Sluiter, J., Templeton, D., Crocker, D., et al. (2008). Determination of structural carbohydrates and lignin in biomass. *Laboratory Analytical Procedure*, *1617*(1), 1–16.

Solomou, K., Alyassin, M., Angelis-Dimakis, A., & Campbell, G. M. (2022). Arabinoxylans: A new class of food ingredients arising from synergies with biorefining, and illustrating the nature of biorefinery engineering. *Food and Bioproducts Processing*, *132*, 83–98. http://dx.doi.org/10.1016/j.fbp.2021.12.007.

Theander, O., & Westerlund, E. A. (1986). Studies on dietary fiber. 3. Improved procedures for analysis of dietary fiber. *Journal of Agricultural and Food Chemistry*, *34*(2), 330–336.

Thompson, C. J., & Ryan, A. J. (2025). Chapter 11 - introduction to polymers: Static scattering. In P. Lindner, & J. Oberdisse (Eds.), *Neutrons, x-rays, and light (second edition)* (2nd ed.). (pp. 285–310). Elsevier, http://dx.doi.org/10.1016/B978-0-443-29116-6.00009-6.

Westberry, B. P., Mansel, B. W., Ryan, T. M., Lundin, L., & Williams, M. (2022). X-ray scattering and molecular dynamics simulations reveal the secondary structure of κ-carrageenan in the solution state. *Carbohydrate Polymers*, *296*, Article 119958. http://dx.doi.org/10.1016/j.carbpol.2022.119958.

Yang, J., & Sato, T. (2020). Conformation of pullulan in aqueous solution studied by small-angle X-ray scattering. *Polymers*, *12*(6), http://dx.doi.org/10.3390/polym12061266.

Yu, L., Yakubov, G. E., Martínez-Sanz, M., Gilbert, E. P., & Stokes, J. R. (2018). Rheological and structural properties of complex arabinoxylans from plantago ovata seed mucilage under non-gelled conditions. *Carbohydrate Polymers*, *193*, 179–188. http://dx.doi.org/10.1016/j.carbpol.2018.03.096.